

<https://doi.org/10.1038/s42949-024-00152-1>

Diversified evolutionary patterns of surface urban heat island in new expansion areas of 31 Chinese cities

Check for updates

Jian Peng¹ , Ruilin Qiao², Qi Wang², Shuying Yu¹, Jianquan Dong^{1,3} & Zhiwei Yang¹

As a hot area of population inflow in the process of urbanization, the urban expansion area faces rapid growth of surface urban heat island (SUHI). However, the multi-dimensional evolutionary characteristics of SUHI in urban expansion areas are still unclear. Through analyzing the evolution of SUHI range ratio, mean intensity and maximum intensity, in this study we identified the comprehensive evolutionary pattern of summer SUHI in urban expansion areas of 31 major cities in China during 2000–2018, and further investigated the corresponding dominant influencing factors. The results showed that the SUHI range and intensity in urban expansion areas exhibited a significant increasing trend in 81% and 71% of the cities respectively during the summer daytime. The cities with declining SUHI range and intensity were distributed in northwestern high-altitude areas with low economic level, while the cities with dominant increases in the SUHI range were distributed in eastern low-altitude areas with high economic level. Climate conditions and population distribution were the dominant influencing factors of intensity-dominated increasing and balanced increasing types, respectively. The intensity and range two-dimensional increasing type had experienced the most severe SUHI growth, with large proportion of secondary industry as the main influencing factor. This study highlighted the importance of multi-dimensional characteristics of SUHI evolution, which provided a new insight to understand SUHI change in urban expansion areas and associated mitigation measures.

The world is urbanizing at an unprecedented rate, with nearly 68% of the global population expected to live in urban areas by 2050¹. Rapid urbanization is accompanied by the continuous expansion of urban landscape and dramatically transforms natural and semi-natural surfaces into artificial surfaces, which intensifies the urban heat island (UHI) effect^{2,3}. With the development of remote sensing technology, satellite-derived surface urban heat island (SUHI) has received more attentions^{4–6}. A better understanding and monitoring of the SUHI is critically important for developing urban heat mitigation strategies.

As a concentrated area for the transformation of non-urban landscape into urban landscape during urbanization, urban expansion area faces rapid growth of SUHI^{7,8}. It has been proven that the SUHI growth trend of urban expansion areas is more prominent than that of old urban areas⁹. Over time, the urban high-temperature center has gradually dispersed from the old urban area to the new expansion area¹⁰. Thus, it is necessary to carry out the long-term monitoring and

corresponding driving force research of SUHI in urban expansion areas.

The spatiotemporal dynamic evolution of SUHI is the key content of urban thermal environment monitoring. Many scholars have reported that the SUHI is increasing with the continuous improvement of urbanization^{11–13}. In general, it can be concluded that the increase in SUHI is mainly manifested in two aspects: intensity^{14,15} and range/footprint^{16,17}. However, these two situations do not always occur simultaneously. For instance, the SUHI intensity of summer daytime in Fuzhou, China, increased from 2000 to 2015, while its footprint decreased slightly from 2003 to 2016; On the contrary, the SUHI footprint in Shanghai showed a significant increasing trend, while its intensity decreased^{12,18}. The specific growth direction of SUHI is vital for urban thermal environment mitigation, which is rarely explored in previous studies. Therefore, it is necessary to pay attention to the multi-dimensional characteristics of SUHI evolution and thus identify comprehensive evolutionary patterns.

¹Laboratory for Earth Surface Processes, Ministry of Education, College of Urban and Environmental Sciences, Peking University, Beijing, China. ²Key Laboratory for Environmental and Urban Sciences, School of Urban Planning and Design, Shenzhen Graduate School, Peking University, Shenzhen, China. ³School of Landscape Architecture, Beijing Forestry University, Beijing, China. ✉e-mail: jianpeng@urban.pku.edu.cn

It is known that the spatiotemporal evolutionary characteristics of SUHI are affected by lots of social or ecological factors, mainly including climate conditions^{19,20}, geographical location^{21,22}, socioeconomic condition^{23,24}, landscape type^{21,25}, and urban morphology^{26,27}. Generally, the influencing factors involved in previous studies are relatively comprehensive, but most of them only discussed the dominant influencing factors of the temporal trend of a certain dimension, rather than integrating the attribution analysis of the multi-dimensional SUHI evolutionary characteristics. This study aims to explore the comprehensive evolution characteristics of SUHI in urban expansion areas in the process of rapid urbanization, and the focus on its dominant influencing factors will help to develop urban thermal environment mitigation strategies.

Since the beginning of the 21st century, China has accelerated urban expansion under the context of rapid globalization and socioeconomic development. From 2000 to 2018, the urbanization rate increased from 36.22% to 59.58%, and the urban land expanded from 42600 km² to 74800 km²^{28,29}. Rapid urban expansion has significantly exacerbated the SUHI effect²³. Therefore, in this study, we conducted a comprehensive and detailed analysis of the SUHI evolutionary pattern and driving factors in urban expansion areas of 31 Chinese cities. In detail, the main purposes of the study were: (1) to identify and quantify the SUHI in urban expansion areas during 2000–2018; (2) to explore the evolutionary characteristics of SUHI from three aspects, i.e., range, mean intensity, and maximum intensity; and (3) to determine the comprehensive evolutionary pattern of SUHI as well as their dominant factors.

Results

SUHI change trends in urban expansion areas

Three representative indicators, including the SUHI range ratio (SUHI_Ra), mean intensity (SUHII_Mean), and maximum intensity (SUHII_Max), were applied to monitor the characteristics of SUHI in multiple dimensions. In detail, SUHI_Ra is defined as the ratio of the SUHI range in the urban

expansion area to the SUHI range in the whole urban area. SUHII_Mean and SUHII_Max are the mean and maximum SUHI intensity of all pixels in the urban expansion area, respectively. Figure 1 shows the multi-year average of SUHI_Ra, SUHII_Mean, and SUHII_Max in urban expansion areas of 31 Chinese cities in the summer of 2000–2018. It could be found that the SUHI_Ra varied greatly in different cities, with a higher value in southeastern cities during the daytime and in central cities during the nighttime. Moreover, the SUHI_Ra in the urban expansion area of Hangzhou was the highest whenever it was daytime or nighttime, with value of 60% and 43%, respectively. The SUHII_Mean and SUHII_Max of 31 cities indicated a similar spatial distribution. Specifically, during the daytime, the eastern cities showed higher SUHI intensity, and Urumqi in the northwest also showed extremely high value. During the nighttime, the difference between cities became smaller, and the central and northwestern cities showed relatively higher SUHI intensity. Generally, the values of SUHI_Ra, SUHII_Mean, and SUHII_Max during the daytime were all higher than that during the nighttime.

The SUHI change trend and corresponding significance in urban expansion areas based on linear regression analysis were presented in Fig. 2. As for SUHI_Ra, there were 25 cities (81% of the cities) demonstrating a significant increasing trend during the daytime, and Wuhan showed the highest change rate of 2.69%·yr⁻¹. During the nighttime, a significant increasing trend was observed in 20 cities (65% of the cities), with the highest value of 1.09%·yr⁻¹ in Beijing. As for SUHII_Mean, 22 and 16 cities (71% and 52% of the cities) showed a significant increasing trend during the daytime and nighttime respectively, while the change rate during the nighttime only varied between 0 and 0.05 °C yr⁻¹. As for SUHII_Max, 22 cities (71% of the cities) showed a significant increasing trend during the daytime, and the higher change rate was found in the southeastern cities. However, only 14 cities (45% of the cities) showed a significant increasing trend during the nighttime, with the change rate below 0.1 °C yr⁻¹. In conclusion, the evolutionary trend during the nighttime was not as

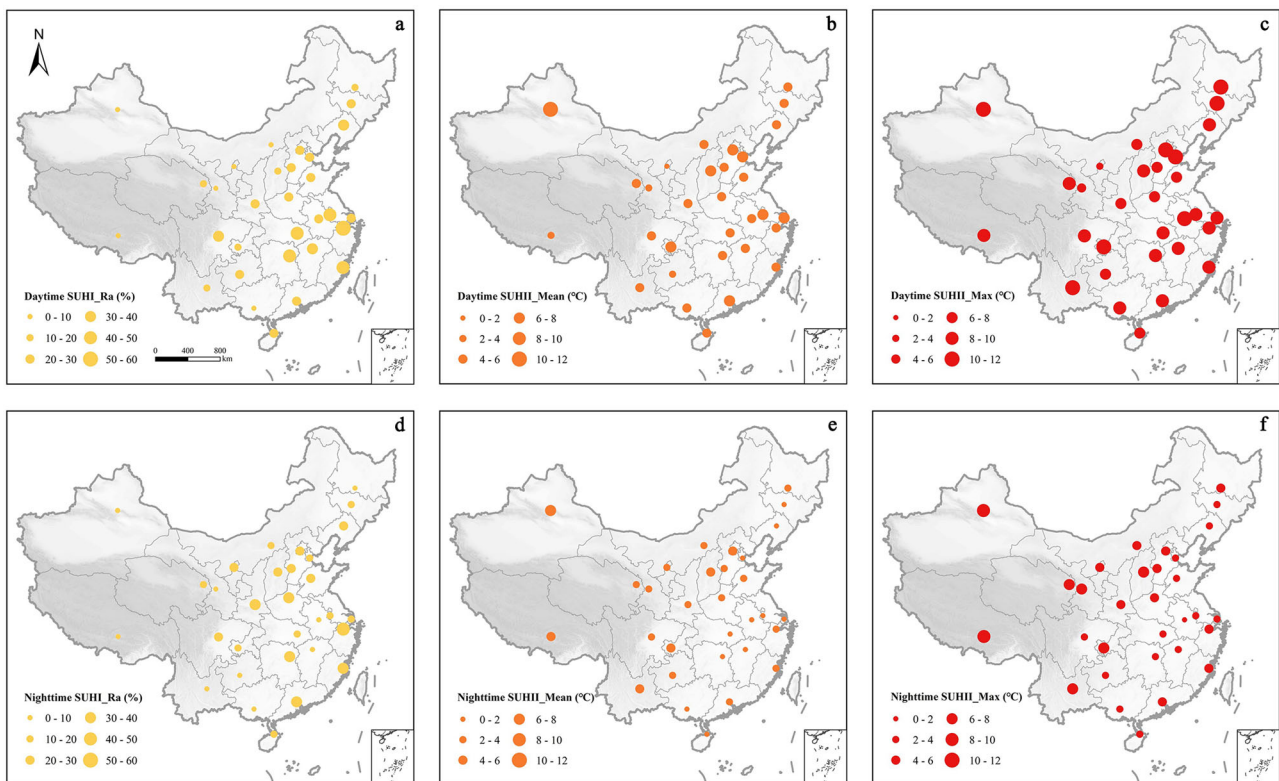


Fig. 1 | Spatial distribution of multi-year average SUHI characteristics in urban expansion areas across 31 Chinese cities from 2000 to 2018. a SUHI_Ra during the daytime. **b** SUHII_Mean during the daytime. **c** SUHII_Max during the daytime.

d SUHI_Ra during the nighttime. **e** SUHII_Mean during the nighttime. **f** SUHII_Max during the nighttime.

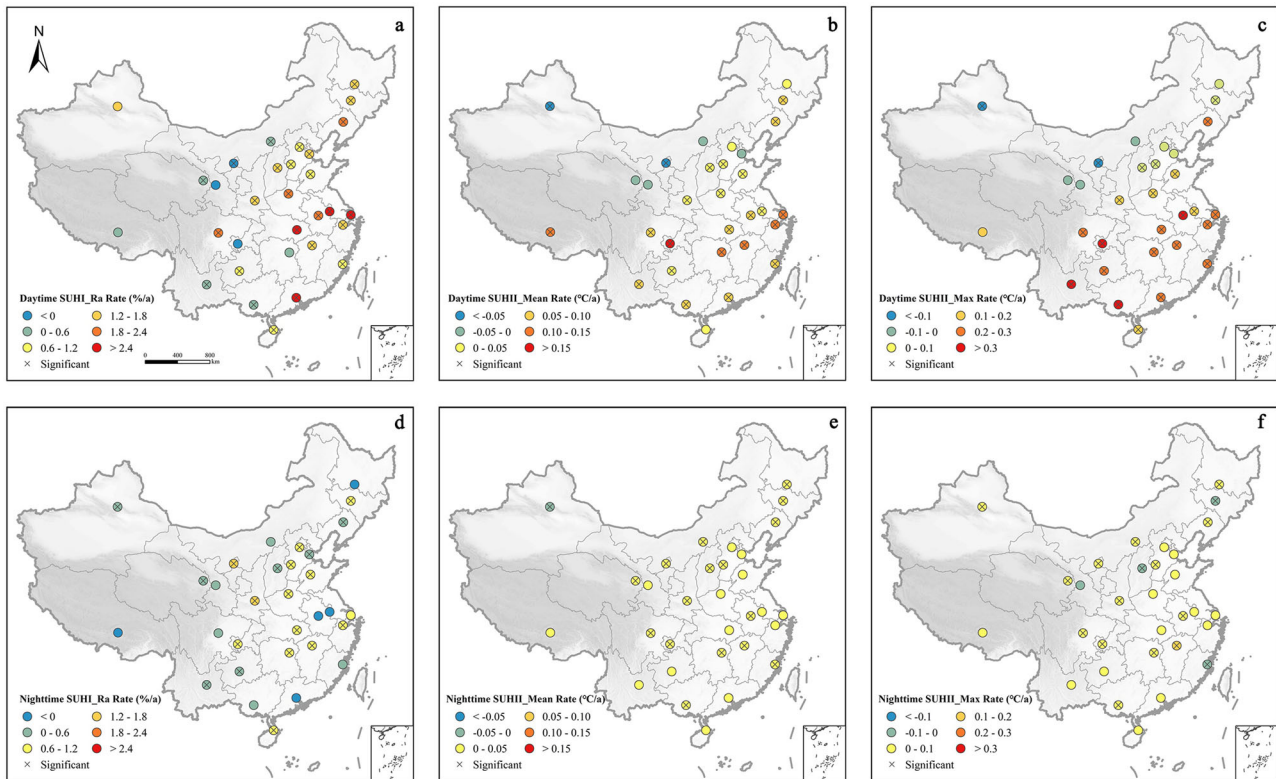


Fig. 2 | Change trend and significance of SUHI characteristic in urban expansion areas across 31 Chinese cities during 2000–2018. a SUHI_Ra during the daytime. **b** SUHII_Mean during the daytime. **c** SUHII_Max during the daytime. **d** SUHI_Ra during the nighttime. **e** SUHII_Mean during the nighttime. **f** SUHII_Max during the nighttime. The color of the points represents change rate, and the cross markers on the points indicate significance at the 0.05 level.

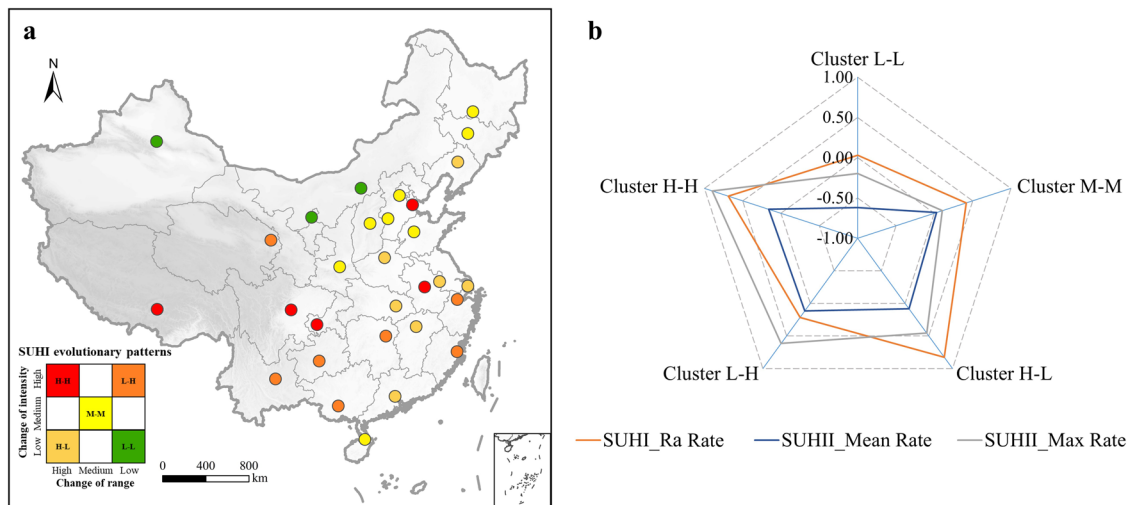


Fig. 3 | SUHI evolutionary patterns of the new expansion areas. a City classification based on the SUHI change trend. **b** Radar diagram of normalized eigenvalues of each cluster center.

significant as that during the daytime in any dimension, and it exhibited inconspicuous diversity among 31 cities during the nighttime. Therefore, more attentions were further paid to the evolutionary pattern of SUHI in urban expansion areas during the summer daytime.

SUHI evolutionary pattern in urban expansion areas

Based on the multi-dimensional evolutionary rates of SUHI in urban expansion areas during summer daytime, these cities were divided into 5 types using the K-means clustering method (Fig. 3). Lanzhou was not included in the classification scheme because the change trends of all three

SUHI characteristics were not significant. The five types can be characterized as follows:

Cluster L-L: Declining type, distributed in northwestern China. The change of SUHI_Ra in urban expansion areas was insignificant, significant decrease, or significantly low increase, while the SUHII_Mean and SUHII_Max were declining. In other words, the evolutionary rates of SUHI range and intensity were both at low levels.

Cluster M-M: Balanced increasing type, mostly located in the north of China, together with Haikou. These cities experienced a balanced increase in the SUHI_Ra, SUHII_Mean, and SUHII_Max in urban expansion areas.

The evolutionary rates of SUHI range and intensity were both at medium levels.

Cluster H-L: Range-dominated increasing type, mostly distributed in the east of China. Compared with SUHI_Mean and SUHI_Max, the SUHI_Ra has experienced an increase at higher rate. The evolutionary rate of SUHI range was at high level, while the evolutionary rate of SUHI intensity was at lower level.

Cluster L-H: Intensity-dominated increasing type, mainly located in the south of China. The evolutionary rate of SUHI intensity was at high level, while the evolutionary rate of SUHI range was at relatively low level, which was the opposite of range-dominated increasing type.

Cluster H-H: Two-dimensional increasing type, mostly distributed in the central part. They experienced a significant increase in the SUHI_Ra,

SUHI_Mean, and SUHI_Max. The evolutionary rates of SUHI range and intensity were both at high levels.

It could be concluded that the urban expansion areas of declining type cities and two-dimensional increasing type cities have experienced the gentlest and most dramatic SUHI growth, respectively, while the growth of balanced increasing type cities was between the two types. For the range-dominated/intensity-dominated increasing type cities, it is necessary to focus on the prominent single-dimensional SUHI growth trend.

Dominant driving factors of SUHI evolution patterns

20 indicators involved environmental background (elevation, precipitation, temperature, latitude, and longitude), urban landscape (area proportion of gray/green/blue space, as well as their change rate), and socio-economic factors (GDP, population density, and nighttime light intensity, as well as their change rate; and proportion of primary, secondary, and tertiary industrial output), were selected to explore the important influencing factors of SUHI evolutionary patterns in urban expansion areas. By applying the principal component analysis method to eliminate the multicollinearity among 20 indicators, 7 principal components were acquired, with the cumulative variance contribution rate of more than 80% (Table 1). It should also be noted that only two indicators were not included, i.e., average area proportion of green space in urban expansion area in 2000 and 2018, and the change rate of area proportion of blue space in urban expansion areas from 2000 to 2018, both of which could be represented by the other space related indicators.

As shown in Fig. 4, for the declining type, FAC1 (GDP_M, DEM, Lon, and GDP_R) showed the highest importance score, suggesting that it was the dominant factor influencing this evolutionary pattern. The economy of these northwest high-altitude cities was at a low level but had grown rapidly. The economic development might be concentrated in old urban areas, which contributed to the decline of UHI in urban expansion areas. The dominant factor affecting the balanced increasing type was FAC4 (PD_M, Light_M, and Grey_M), which implied that the synergy of population growth and landscape urbanization in new expansion areas could tend to the formation of the balanced increasing type SUHI. For the range-dominated increasing type, the dominant factor was the same as the declining type. But on the contrary, such cities were generally closer to coastal areas with lower altitudes. Their economy was at a high level but had

Table 1 | Principal component factors and corresponding representative indicators

Factor	Definition	Representative Indicators
FAC 1	Economy-dominated	GDP_M (-0.86 [*]), DEM (0.84 [*]), Lon (-0.81 [*]), GDP_R (0.71 [*])
FAC 2	Climate-dominated	Prep (0.91 [*]), Lat (-0.87 [*]), Tem (0.86 [*])
FAC 3	Industry-dominated	PSI (0.91 [*]), PTI (-0.89 [*]), Light_R (0.82 [*])
FAC 4	Population-dominated	PD_M (0.79 [*]), Light_M (0.79 [*]), Grey_M (0.73 [*])
FAC 5	Population-industry-dominated	PD_R (0.88 [*]), PPI (-0.86 [*])
FAC 6	Landscape-dominated	Green_R (-0.77 [*]), Grey_R (0.75 [*])
FAC 7	Water-dominated	Blue_M (0.82 [*])

^{*}represents the significance at 0.01 level (two-tailed). DEM, average DEM of urban expansion area; Prep, multi-year average precipitation of urban expansion area; Tem, multi-year average temperature of urban expansion area; Lat, latitude of the city center; Lon, longitude of the city center; Grey_M and Blue_M, average area proportion of gray/blue space in urban expansion area in 2000 and 2018, respectively; Grey_R and Green_R, change rate of area proportion of gray/green space in urban expansion area from 2000 to 2018, respectively; PD_M, Light_M, and GDP_M, average population density, nighttime light intensity and GDP in urban expansion area in 2000 and 2018, respectively; PD_R, Light_R, and GDP_R, the change rate of population density, nighttime light intensity and GDP in urban expansion area from 2000 to 2018, respectively; and PPI, PSI, and PTI, the proportion of primary, secondary and tertiary industrial output of the city in 2018, respectively.

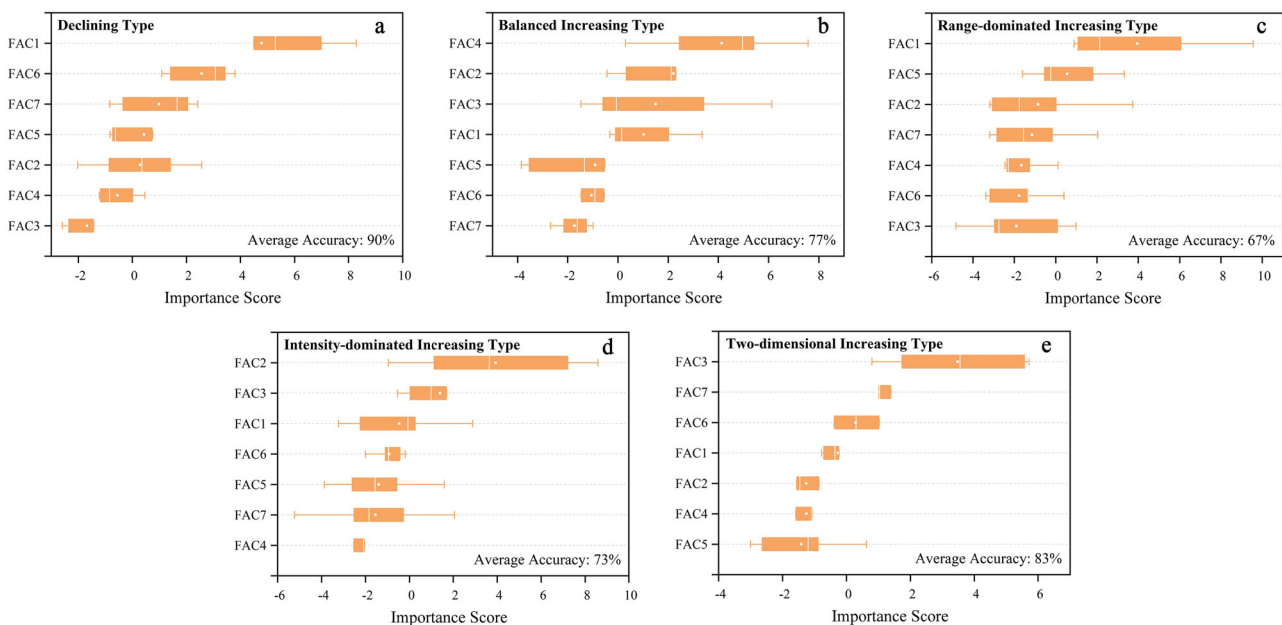


Fig. 4 | Boxplot of variable importance scores for five UHI evolution patterns based on 5-fold cross-validation of RF model. a Declining type. b Balanced increasing type. c Range-dominated increasing type. d Intensity-dominated type. e Two-dimensional increasing type.

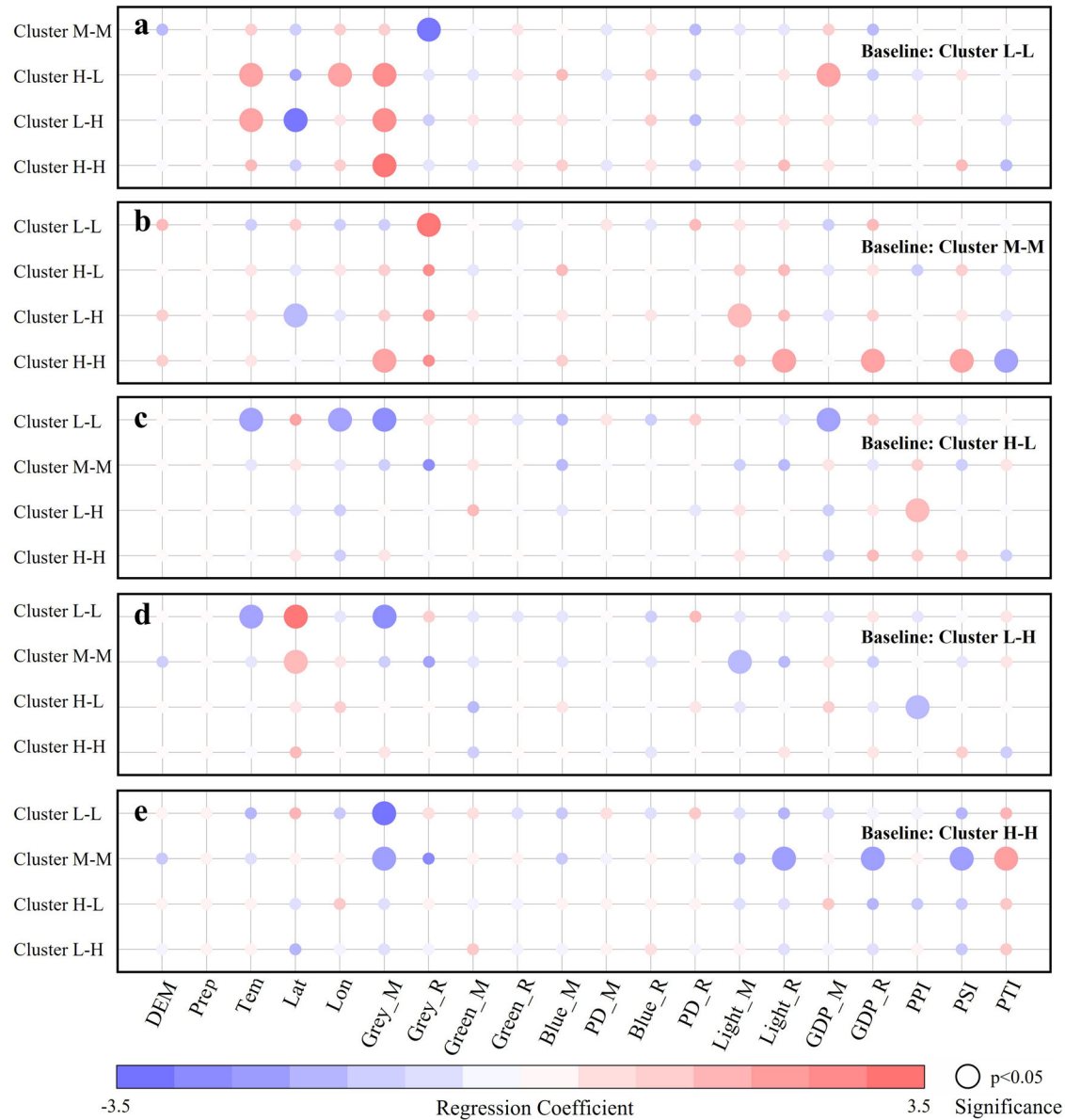


Fig. 5 | Regression coefficients and their significance of the multinomial logistic regression with different cluster as the baseline. a Declining type (Cluster L-L) as the baseline. **b** Balanced increasing type (Cluster M-M) as the baseline. **c** Range-dominated increasing type (Cluster H-L) as the baseline. **d** Intensity-dominated

increasing type (Cluster L-H) as the baseline. **e** Two-dimensional increasing type (Cluster H-H) as the baseline. The color and size of points represent the regression coefficient and the corresponding significance, respectively.

grown less, which might occur in urban expansion areas, leading to the continuous increase of SUHI range. FAC2 (Prep, Lat, and Tem) was the dominant factor affecting the intensity-dominated increasing type. The lower latitude, as well as the climate characteristics of warm and humid, contributed to the formation of this evolutionary pattern. For the two-dimensional increasing type, FAC3 (PSI, PTI, and Light_R) was the dominant influencing factor, indicating that a high proportion of the secondary industry was the key to the formation of this evolutionary pattern.

In order to explore key driving factors that can potentially change the SUHI evolutionary pattern of the urban expansion area, the multinomial logistic regression model was further applied with each pattern as the baseline respectively (Fig. 5). Taking the balanced increasing type (Cluster M-M) as the baseline as an example, the SUHI evolutionary pattern was inclined to develop into the declining type (Cluster L-L) when the change rate of area proportion of gray space was higher. In other words, the declining type cities might have a higher change rate of area proportion of gray space, but their SUHI showed a declining trend. As a result, the spatial

configuration of gray space deserve further attentions. When the latitude was lower and the nighttime light intensity representing the socioeconomic development level was higher, the balanced increasing type tended to develop into the intensity-dominated increasing type (Cluster L-H), meaning a significant increase in SUHI intensity. Moreover, when the area proportion of gray space and both change rates of nighttime light intensity and GDP in urban expansion areas were higher, and the urban industrial structure was more inclined to secondary industry, this pattern tended to develop into the two-dimensional increasing type (Cluster H-H).

Discussion

As the first choice to relieve human pressure on the old urban area, the new urban expansion area is a crucial approach in the urbanization process, which guides urban growth and provides alternative solution for urban development⁷. Previous studies have demonstrated that the warming was more prominent in urban expansion areas than in old urban areas^{9,30,31}. If the study on the evolutionary trend of SUHI is only carried out from the

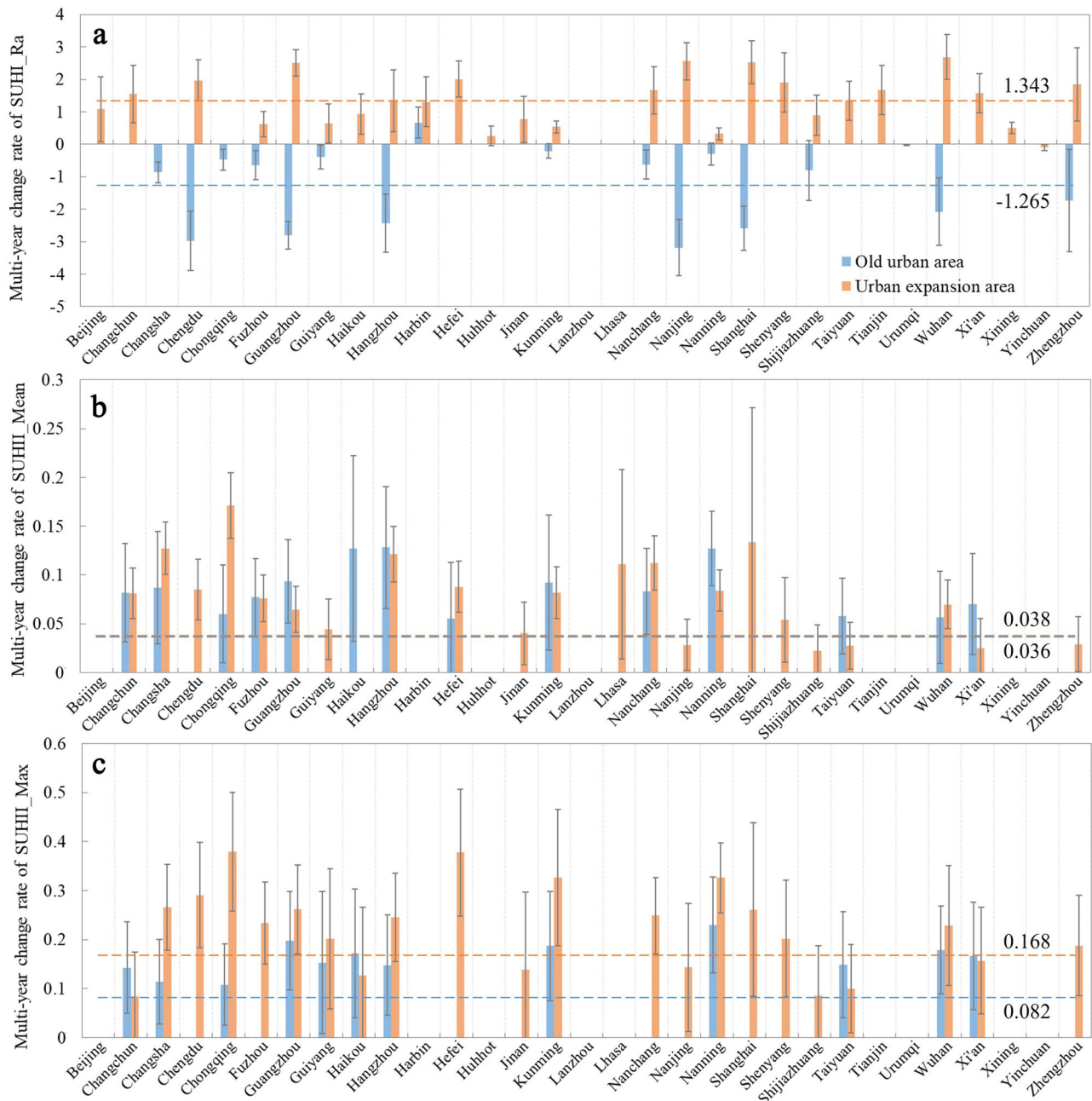


Fig. 6 | Comparison of the multi-year change rate of SUHI in the old urban area and urban expansion area. a SUHI_Ra. **b** SUHII_Mean. **c** SUHII_Max. Cities that passed the significance test are shown (**b**, **c** only show cities with significant

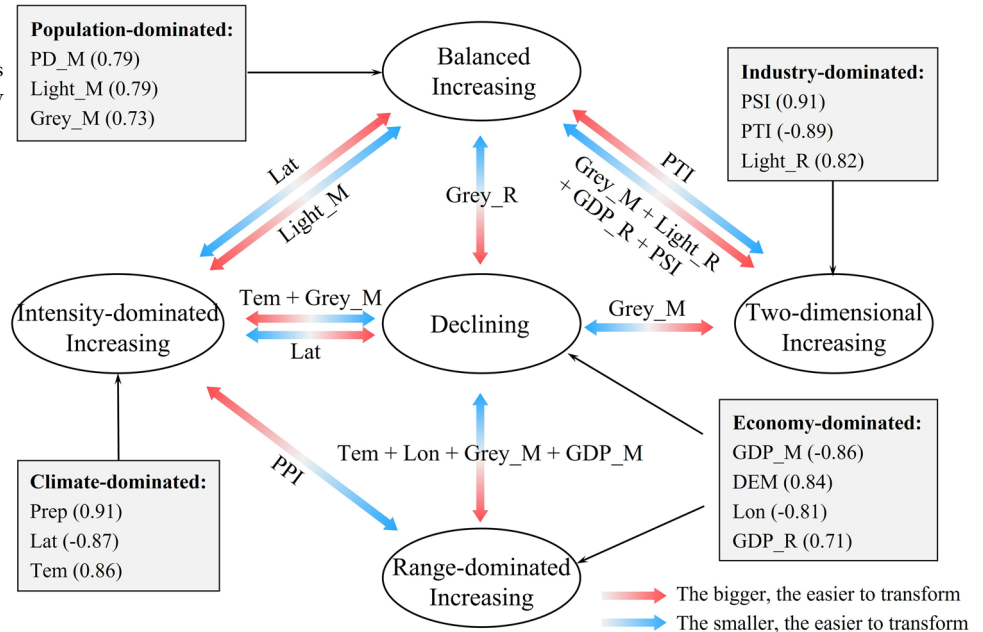
increases), the error bar represents the standard error of the change rate, and horizontal lines represent the average values.

perspective of the whole urban area, its increasing trend may be underestimated. Taking the study of Zhou et al.³² as an example, the significant increasing trend of summer daytime SUHI intensity was observed in about one-third of the 32 major Chinese cities³². However, this trend was found in urban expansion areas of about 71% of cities in our study. To verify the necessity of focusing on the long-term evolutionary pattern of SUHI in urban expansion areas, we further compared the evolutionary characteristics of summer daytime SUHI in old urban areas and urban expansion areas.

As shown in Fig. 6, the average multi-year change rate of SUHI_Ra in old urban areas was negative, much lower than that in urban expansion areas. Specifically, the significant decreasing trend was found in old urban areas of 16 cities, but none in new expansion areas. This result suggested that the SUHI in most cities might gradually shift from the old urban area

to the new expansion area. In terms of the SUHI intensity, the average multi-year change rates of SUHII_Mean and SUHII_Max in urban expansion areas were both higher than that in old urban areas, and only 14 and 12 cities showed a significant increasing trend of SUHII_Mean and SUHII_Max in old urban areas respectively. It could be seen that no matter in which dimension, the increasing trend of SUHI in urban expansion areas was dramatically higher than that in old urban areas. Similar to our results, Yao et al.³³ found that the increasing trend of SUHI intensity in the area converted from other land use types to urban construction land during 2001–2015 was significantly higher than that of the area with stable urban construction land³³. Therefore, studies on the evolutionary characteristics of SUHI in urban expansion areas are crucial for sustainable urban development in view of mitigating SUHI stress in the context of global warming.

Fig. 7 | Changing mechanism of SUHI evolutionary pattern in the urban expansion area. The figure summarizes the dominant influencing factors of various SUHI evolution patterns (marked in gray boxes) and the key drivers of transformation between different patterns (shown on arrows).



In the process of rapid urbanization, most Chinese cities have experienced suburban urbanization between 2000 and 2018, resulting in widespread urban expansion areas²⁹. Through analyzing the dominant influencing factors of the summer daytime SUHI evolutionary pattern and the critical transition drivers between various patterns in urban expansion areas, different evolution mechanisms among various patterns were found (Fig. 7). In the process of urbanization from 2000 to 2018, the SUHI growth and urban construction have developed in the same direction in urban expansion areas of most cities, with the opposite direction only in three cities in this study, namely the declining type cities. The increasing SUHI makes urban expansion areas face more and more thermal risk, especially in two-dimensional increasing type cities and range-dominated or intensity-dominated increasing type cities.

For the control of SUHI in new urban areas, on the one hand, an early warning for the future is important. For instance, declining type cities currently exhibit a low SUHI growth trend, but with the rise of temperature under climate change, they may change to range-dominated or intensity-dominated increasing type. In the face of this possibility in the future, we should pay attention to the optimization of scale and arrangement of gray space in future urban construction³⁴. On the other hand, it is urgent to take measures to alleviate the current SUHI trend. The evolution of SUHI in urban expansion areas of two-dimensional increasing type cities dominated by industrial structure is the most severe, and the transformation and upgrading to the service industry as the leading industry are the keys to change them to the pattern with a lower SUHI growth. Meanwhile, it is also necessary to adopt other SUHI mitigation methods, such as the cooling effect of green space or water body^{35,36}. The urban expansion areas with intensity-dominated increasing of SUHI is confronted with more severe extreme SUHI. Although the environmental background is the dominant factor to form this pattern, controlling the gray landscape area and optimizing the spatial distribution of economic activity areas are meaningful ways to transform it into a pattern with a lower SUHI growth.

This study analyzed the evolutionary characteristics and patterns of SUHI in urban expansion areas of 31 major cities in China from 2000 to 2018 and explored the dominant influencing factors of various evolution patterns and the key drivers of transformation between different evolution patterns. However, there are also some limitations in this study. Firstly, SUHI was identified based on MODIS data. However, there may be bias in the identified SUHI because of the thermal anisotropy, which poses a challenge for precisely calculating the intensity and range of SUHI^{37,38}.

Secondly, due to seasonal differences in the SUHI³⁹, the SUHI evolutionary patterns in urban expansion areas should be explored throughout one year, not just for a single season. Lastly, only the influences of environmental background, urban landscape and socio-economic factors were considered. In the future, more influencing factors can be included, such as urban spatial configuration and urban form, in order to provide a more detailed guidance in urban planning⁴⁰.

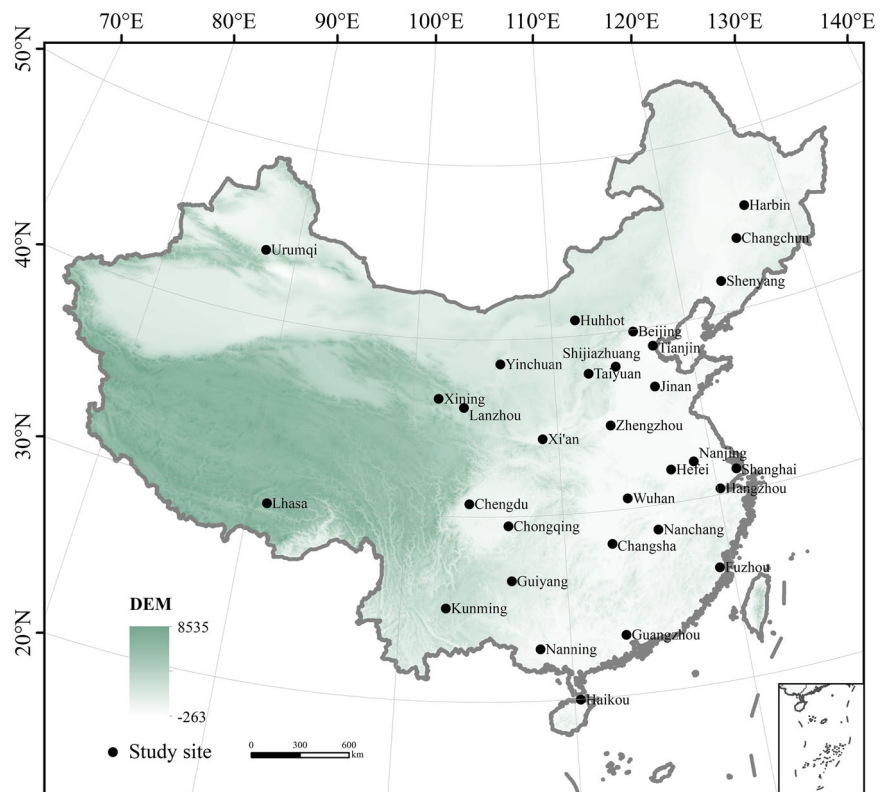
Methods

Study area and data sources

31 major cities in China, including 4 municipalities and 27 provincial capitals, were selected as study areas (Fig. 8). As the political centers of various regions, these cities have continuously expanded their built-up areas during the rapid urbanization process in recent decades. According to the China City Statistical Yearbook, the largest expansion area of urban built-up area is 1349 km² in Shanghai, and the smallest is 34 km² in Xining. Thus, these cities are ideal study areas for exploring the SUHI effect of urban expansion areas.

The main datasets used in this study were as follows: (1) Global Urban Boundaries (GUB), developed by Li et al.⁴¹. We applied this data to extract urban expansion areas of 31 cities and regarded the urban areas before 2000 as old urban areas, and the growth areas of urban areas from 2000 to 2018 as urban expansion areas⁸; (2) 8-day land surface temperature (LST) product MOD11A2, provided by the United States Geological Survey (<https://earthexplorer.usgs.gov/>). We acquired 502 images covering the study areas with a spatial resolution of 1 km from 2000 to 2018 in summer (from June to August). After cloud removal and quality control, the images in July were used to calculate the mean LST of daytime and nighttime, and the images in June and August were used to supplement missing values; (3) land use data during 2000–2018, provided by the Resource and Environment Science and Data Center of the Chinese Academy of Sciences (<https://www.resdc.cn/>), with a spatial resolution of 1 km. The land use includes 6 categories: cropland, forest land, grassland, water area, construction land, and unused land; (4) VIIRS/NPP nighttime light data and DMSP/OLS nighttime light data, acquired from the National Oceanic and Atmospheric Administration (<https://ngdc.noaa.gov/eog/>). Since the DMSP/OLS nighttime light data were not available subsequent to February 2014, in this study we applied the conversion method proposed by Li et al.⁴² to intercalibrate the DMSP/OLS nighttime light data and VIIRS/NPP data⁴²; (5) meteorological data, including the national average annual precipitation and average

Fig. 8 | Location of 31 major cities in China. The center and name of the cities are marked in the figure.



temperature during 2000–2018, provided by the Resource and Environment Science and Data Center of the Chinese Academy of Sciences (<https://www.resdc.cn/>), with a spatial resolution of 1 km; (6) socioeconomic data, including the 1 km grid population density data acquired from the WorldPOP (<https://www.worldpop.org/>) and industrial structure and Gross Domestic Product (GDP) collected from the China statistical year-book; and (7) Digital Elevation Model (DEM), downloaded from the Shuttle Radar Topographic Mission (SRTM) database published by the National Aeronautics and Space Administration (NASA) (<https://eosps.gsf.nasa.gov/>), with a spatial resolution of 30 m.

SUHI quantification

The intensity of SUHI was usually calculated as the difference in land surface temperature between the urban and rural or suburban areas^{15,43}. To monitor multi-year SUHI in urban expansion areas, it is necessary to consider the dynamic changes in the extent of suburban areas. Therefore, in this study we identified the suburban areas according to the following rules: (1) areas outside the old urban area and the urban expansion area in a city; (2) flat fields close to the altitude of urban areas; (3) the land use type was stable as forest land or grassland during 2000–2018; and (4) areas where the DN value of nighttime light was less than or equal to 15 during 2000–2018⁴⁴. The intensity of SUHI can be calculated using Eq. (1).

$$\text{SUHI}_i = \text{LST}_i - \overline{\text{LST}}_{\text{Sub}} \quad (1)$$

In Eq. (1), SUHI_i refers to the surface heat island intensity of pixel i , LST_i is the LST of pixel i , and $\overline{\text{LST}}_{\text{Sub}}$ is the mean of suburban LST.

Then, the percentile-based thermal threshold method proposed by Shreevastava et al.⁴⁵ was used to identify the range of SUHI in urban expansion areas. Specifically, for each city, the value of the top 5% percentile of SUHI intensity in urban areas every year was used as the threshold for identifying the SUHI range. Compared with

selecting a certain fixed value as the threshold for all the cities, this method is beneficial to compare the variation of SUHI in different cities, and to identify multi-year SUHI evolutionary characteristics of the same city.

SUHI evolution analysis

To analyze the temporal evolutionary trend of SUHI in urban expansion areas, the linear regression model based on ordinary least squares was applied to determine the slopes of three indicators over time for each city, which were regarded as the evolutionary rates. In addition, t-test was used to examine the significance of evolutionary rates.

The evolutionary rates of SUHI_{Ra} , $\text{SUHI}_{\text{Mean}}$, and SUHI_{Max} in urban expansion areas were normalized by their respective max absolute value, which were further introduced into the K-means clustering as three features of sample points to classify the types of SUHI evolutionary patterns. K-means clustering can partition n observations into K clusters so that the similarity among samples in the same cluster is higher than that in different clusters. K points in the samples were randomly selected as centroids of K clusters, and all sample points were classified into the nearest cluster according to their distance to each centroid. Then, the centroid of each cluster was recalculated. If the distance between new centroids and original centroids was less than a set threshold, the data has converged, otherwise, the classification schemes would be adjusted by the distance from the centroids until convergence.

Due to the difficulty of determining the cluster number K artificially, in this study we used the elbow method to test the optimal clustering results by observing the variation trend of the sum of squared errors (SSE) with the cluster number K ⁴⁶. The SSE can be calculated as shown in Eq. (2).

$$\text{SSE} = \sum_{i=1}^k \sum_{p \in C_i} |p - m_i|^2 \quad (2)$$

In Eq. (2), C_i is the i^{th} cluster, p represents the samples in C_i , and m_i represents the cluster center of C_i .

Influencing factors identification for SUHI evolutionary pattern

In this study we comprehensively considered the impact of environmental background, urban landscape, and socio-economic factors on the evolutionary pattern of SUHI in urban expansion areas. Generally, environmental background consists of DEM, temperature, and precipitation, as well as longitude and latitude¹⁹. In particular, when cities are located at different longitudes and latitudes, there are diversities in the received solar radiation and the change of solar altitude angle, which may affect the UHI effect²². Thus, they were included in the environmental background factors. Urban landscape considers the area proportions of gray, green, and blue space⁴⁷. Among them, the gray space is construction land, the green space consists of forest land and grassland, and the blue space is water area. Socio-economic factors include population density, nighttime light intensity, industrial structure, and GDP. To make data closer to a normal distribution, the population density and GDP were log-transformed⁴⁸. Finally, all the factors were standardized with Z-Score to ensure uniform magnitude.

To explore the important driving forces affecting the SUHI evolutionary pattern in urban expansion areas, the principal component analysis was firstly applied to reduce the dimensionality of 20 influencing factors and thus to eliminate the multicollinearity among them. Then, taking rotated principal components as explanatory variables, and types of evolutionary pattern as response variable, the random forest (RF) model was used to investigate the relative importance of the impact of each explanatory variable on the SUHI evolutionary pattern. RF model is an algorithm based on a classification tree, in which mean decrease accuracy (MDA) is a key indicator characterizing the relative importance of variables⁴⁹. It quantifies the decrease in prediction accuracy when changing the values of an explanatory variable into random numbers. The larger of MDA is, the more important the variable is. In this study, we used the package ‘randomForest’ in R to implement the RF model. In addition, a 5-fold cross-validation was conducted on the RF model to improve the robustness of the results⁵⁰. Cross-validation randomly divided the training and testing sets to generate different models, and the importance of variables based on the average MDA run by these models.

The multinomial logistic regression model is available when the dependent variable is an unordered categorical variable, which pairs each category with the baseline/reference category, and the mathematical expression is shown in Eq. (3). When the number of categories of the dependent variable is 2, the model is equivalent to binary logistic regression. In this study, with various SUHI evolutionary types as the baseline in turn, the multinomial logistic regression was established to identify the drivers of mutual conversion between different evolutionary patterns in the urban expansion area.

$$g_j(x) = \ln \frac{y_j}{y_0} = \alpha_j + \beta_j x \quad (3)$$

In Eq. (3), y_0 is the baseline category, $g_j(x)$ represents the regression equation for the remaining category y_j paired with the baseline, and α_j and β_j represent the corresponding intercept and regression coefficients respectively.

Reporting summary

Further information on research design is available in the Nature Research Reporting Summary linked to this article.

Data availability

The data used in this study, including global urban boundaries, LST, land use, night light intensity, meteorological variables, socioeconomic variables and DEM were obtained from publicly available data with free access.

Code availability

The code used to produce the results of this study is available from the authors upon reasonable request.

Received: 6 February 2023; Accepted: 2 March 2024;

Published online: 15 March 2024

References

- Sun, L., Chen, J., Li, Q. & Huang, D. Dramatic uneven urbanization of large cities throughout the world in recent decades. *Nat. Commun.* **11**, 5366 (2020).
- Mohajerani, A., Bakaric, J. & Jeffrey-Bailey, T. The urban heat island effect, its causes, and mitigation, with reference to the thermal properties of asphalt concrete. *J. Environ. Manage.* **197**, 522–538 (2017).
- Peng, J., Xie, P., Liu, Y. & Ma, J. Urban thermal environment dynamics and associated landscape pattern factors: a case study in the Beijing metropolitan region. *Remote Sens. Environ.* **173**, 145–155 (2016).
- Lai, J. et al. Meteorological controls on daily variations of nighttime surface urban heat islands. *Remote Sens. Environ.* **253**, 112198 (2021).
- Li, J. et al. Impacts of landscape structure on surface urban heat islands: a case study of Shanghai, China. *Remote Sens. Environ.* **115**, 3249–3263 (2011).
- Manoli, G., Fatichi, S., Bou-Zeid, E. & Katul, G. G. Seasonal hysteresis of surface urban heat islands. *Proc. Natl Acad. Sci. USA* **117**, 7082–7089 (2020).
- Shahraiyni, H. T. et al. A comprehensive statistical study on daytime surface urban heat island during summer in urban areas, case study: Cairo and its new towns. *Remote Sens.* **8**, 643 (2016).
- Zhao, J. et al. Exploring difference in land surface temperature between the city centres and urban expansion areas of China’s major cities. *Int. J. Remote Sens.* **41**, 8963–8983 (2020).
- Wang, J., Zhou, W. & Wang, J. Time-series analysis reveals intensified urban heat island effects but without significant urban warming. *Remote Sens.* **11**, 2229 (2019).
- Shen, H., Huang, L., Zhang, L., Wu, P. & Zeng, C. Long-term and fine-scale satellite monitoring of the urban heat island effect by the fusion of multi-temporal and multi-sensor remote sensed data: a 26-year case study of the city of Wuhan in China. *Remote Sens. Environ.* **172**, 109–125 (2016).
- Chapman, S., Watson, J. E. M., Salazar, A., Thatcher, M. & McAlpine, C. A. The impact of urbanization and climate change on urban temperatures: A systematic review. *Landsc. Ecol.* **32**, 1921–1935 (2017).
- Ren, T., Zhou, W. & Wang, J. Beyond intensity of urban heat island effect: a continental scale analysis on land surface temperature in major Chinese cities. *Sci. Total Environ.* **791**, 148334 (2021).
- Ramsay, E. E. et al. Spatio-temporal development of the urban heat island in a socioeconomically diverse tropical city. *Environ. Pollut.* **316**, 120443 (2023).
- Dewan, A. et al. Surface urban heat island intensity in five major cities of Bangladesh: patterns, drivers and trends. *Sustain. Cities Soc.* **71**, 102926 (2021).
- Si, M. et al. Spatiotemporal pattern and long-term trend of global surface urban heat islands characterized by dynamic urban-extent method and MODIS data. *ISPRS J. Photogramm. Remote Sens.* **183**, 321–335 (2022).
- Yao, L. et al. Understanding the spatiotemporal pattern of the urban heat island footprint in the context of urbanization, a case study in Beijing, China. *Appl. Geogr.* **133**, 102496 (2021).
- Peng, J., Hu, Y., Dong, J., Liu, Q. & Liu, Y. Quantifying spatial morphology and connectivity of urban heat islands in a megacity: a radius approach. *Sci. Total Environ.* **714**, 136792 (2020).

18. Yang, Q., Huang, X. & Tang, Q. The footprint of urban heat island effect in 302 Chinese cities: temporal trends and associated factors. *Sci. Total Environ.* **655**, 652–662 (2019).
19. Zhao, L., Lee, X., Smith, R. B. & Oleson, K. Strong contributions of local background climate to urban heat islands. *Nature* **511**, 216–219 (2014).
20. Song, Z. et al. The spatiotemporal pattern and influencing factors of land surface temperature change in China from 2003 to 2019. *Int. J. Appl. Earth Obs. Geoinf.* **104**, 102537 (2021).
21. Peng, J., Jia, J., Liu, Y., Li, H. & Wu, J. Seasonal contrast of the dominant factors for spatial distribution of land surface temperature in urban areas. *Remote Sens. Environ.* **215**, 255–267 (2018).
22. Thiery, W. et al. Warming of hot extremes alleviated by expanding irrigation. *Nat. Commun.* **11**, 290 (2020).
23. Manoli, G. et al. Magnitude of urban heat islands largely explained by climate and population. *Nature* **573**, 55–60 (2019).
24. Fu, X., Yao, L., Xu, W., Wang, Y. & Sun, S. Exploring the multitemporal surface urban heat island effect and its driving relation in the Beijing-Tianjin-Hebei urban agglomeration. *Appl. Geogr.* **144**, 102714 (2022).
25. Gao, J., Gong, J., Yang, J., Li, J. & Li, S. Measuring spatial connectivity between patches of the heat source and sink (SCSS): a new index to quantify the heterogeneity impacts of landscape patterns on land surface temperature. *Landsc. Urban Plan.* **217**, 104260 (2022).
26. Li, Y., Schubert, S., Kropp, J. P. & Rybski, D. On the influence of density and morphology on the Urban Heat Island intensity. *Nat. Commun.* **11**, 1–9 (2020).
27. Logan, T. M., Zaitchik, B., Guikema, S. & Nisbet, A. Night and day: the influence and relative importance of urban characteristics on remotely sensed land surface temperature. *Remote Sens. Environ.* **247**, 111861 (2020).
28. Bai, X., Shi, P. & Liu, Y. Realizing China's urban dream. *Nature* **509**, 158–160 (2014).
29. Kuang, W. 70 years of urban expansion across China: Trajectory, pattern, and national policies. *Sci. Bull.* **65**, 1970–1974 (2020).
30. Liu, Z. et al. Surface warming in global cities is substantially more rapid than in rural background areas. *Commun. Earth Environ.* **3**, 219 (2022).
31. Zhou, W. et al. Beyond city expansion: Multi-scale environmental impacts of urban megaregion formation in China. *Natl. Sci. Rev.* **9**, nwab107 (2022).
32. Zhou, D. et al. Spatiotemporal trends of urban heat island effect along the urban development intensity gradient in China. *Sci. Total Environ.* **544**, 617–626 (2016).
33. Yao, R. et al. Temporal trends of surface urban heat islands and associated determinants in major Chinese cities. *Sci. Total Environ.* **609**, 742–754 (2017).
34. Han, S., Li, W., Kwan, M. P., Miao, C. & Sun, B. Do polycentric structures reduce surface urban heat island intensity? *Appl. Geogr.* **146**, 102766 (2022).
35. Cheng, Y. et al. How to use lake breeze circulations to improve urban natural ventilation: a case study in a typical inland multi-lake megacity. *Landsc. Urban Plan.* **230**, 104628 (2023).
36. Peng, J. et al. How to effectively mitigate urban heat island effect? A perspective of waterbody patch size threshold. *Landsc. Urban Plan.* **202**, 103873 (2020).
37. Hu, L., Monaghan, A., Voogt, J. A. & Barlage, M. A first satellite-based observational assessment of urban thermal anisotropy. *Remote Sens. Environ.* **181**, 111–121 (2016).
38. Du, H. et al. Global mapping of urban thermal anisotropy reveals substantial potential biases for remotely sensed urban climates. *Sci. Bull.* **68**, 1809–1818 (2023).
39. Hu, Y., Dai, Z. & Guldmann, J. M. Modeling the impact of 2D/3D urban indicators on the urban heat island over different seasons: a boosted regression tree approach. *J. Environ. Manage.* **266**, 110424 (2020).
40. Yang, J., Xin, J., Zhang, Y., Xiao, X. & Xia, J. C. Contributions of sea-land breeze and local climate zones to daytime and nighttime heat island intensity. *npj Urban Sustain.* **2**, 1–11 (2022).
41. Li, X. et al. Mapping global urban boundaries from the global artificial impervious area (GAIA) data. *Environ. Res. Lett.* **15**, 094044 (2020).
42. Li, X., Li, D., Xu, H. & Wu, C. Intercalibration between DMSP/OLS and VIIRS night-time light images to evaluate city light dynamics of Syria's major human settlement during Syrian Civil War. *Int. J. Remote Sens.* **38**, 5934–5951 (2017).
43. Peng, S. et al. Surface urban heat island across 419 global big cities. *Environ. Sci. Technol.* **46**, 696–703 (2012).
44. Liu, Y., Fang, X., Xu, Y., Zhang, S. & Luan, Q. Assessment of surface urban heat island across China's three main urban agglomerations. *Theor. Appl. Climatol.* **133**, 473–488 (2018).
45. Shreevastava, A., Rao, P. S. C. & McGrath, G. S. Emergent self-similarity and scaling properties of fractal intra-urban heat islets for diverse global cities. *Phys. Rev. E.* **100**, 032142 (2019).
46. Lin, Y. et al. Fine-scale mapping of urban ecosystem service demand in a metropolitan context: a population-income-environmental perspective. *Sci. Total Environ.* **781**, 146784 (2021).
47. Peng, J. et al. Spatial-temporal change of land surface temperature across 285 cities in China: an urban-rural contrast perspective. *Sci. Total Environ.* **635**, 487–497 (2018).
48. Liang, Z. et al. The relationship between urban form and heat island intensity along the urban development gradients. *Sci. Total Environ.* **708**, 135011 (2020).
49. Wu, H., Lin, A., Xing, X., Song, D. & Li, Y. Identifying core driving factors of urban land use change from global land cover products and POI data using the random forest method. *Int. J. Appl. Earth Obs. Geoinf.* **103**, 102475 (2021).
50. Xu, Q. S. & Liang, Y. Z. Monte Carlo cross validation. *Chemometr. Intell. Lab.* **56**, 1–11 (2001).

Acknowledgements

This research was financially supported by the National Natural Science Foundation of China (No. 42130505).

Author contributions

Conceptualization was formulated by J.P. and R.Q. Data collection, analyses, and initial manuscript was performed by R.Q., J.P., and Q.W. S.Y., J.D., and Z.Y. revised article critically for important intellectual content. All authors read and approved the final manuscript.

Competing interests

The authors declare no competing interests.

Additional information

Supplementary information The online version contains supplementary material available at <https://doi.org/10.1038/s42949-024-00152-1>.

Correspondence and requests for materials should be addressed to Jian Peng.

Reprints and permissions information is available at <http://www.nature.com/reprints>

Publisher's note Springer Nature remains neutral with regard to jurisdictional claims in published maps and institutional affiliations.

Open Access This article is licensed under a Creative Commons Attribution 4.0 International License, which permits use, sharing, adaptation, distribution and reproduction in any medium or format, as long as you give appropriate credit to the original author(s) and the source, provide a link to the Creative Commons licence, and indicate if changes were made. The images or other third party material in this article are included in the article's Creative Commons licence, unless indicated otherwise in a credit line to the material. If material is not included in the article's Creative Commons licence and your intended use is not permitted by statutory regulation or exceeds the permitted use, you will need to obtain permission directly from the copyright holder. To view a copy of this licence, visit <http://creativecommons.org/licenses/by/4.0/>.

© The Author(s) 2024